Scanning Kelvin probe force microscopy study of the effect of thermal oxide layers on the hydrogen release - Experiments and finite element method modelling

Tim Rubben, Tom Depover, Kim Verbeken, Reynier I Revilla, Vincent Barnier, Alixe Dreano, Frédéric Christien, Iris de Graeve

INTERNATIONAL JOURNAL OF HYDROGEN ENERGY 48 (2023) 34067–34076

Available online at www.sciencedirect.com

ScienceDirect

journal homepage: www.elsevier.com/locate/he

Scanning Kelvin probe force microscopy study of the effect of thermal oxide layers on the hydrogen release - Experiments and finite element method modelling

Tim Rubben [a,b,*], *Tom Depover* [b], *Kim Verbeken* [b], *Reynier I. Revilla* [a], *Vincent Barnier* [c], *Alixe Dreano* [c], *Frédéric Christien* [c], *Iris De Graeve* [a,b]

[a] *Department of Chemistry and Materials, Vrije Universiteit Brussel (VUB), Research Group of Electrochemical and Surface Engineering (SURF), Pleinlaan 2, 1050, Brussels, Belgium*

[b] *Department of Materials, Textiles and Chemical Engineering, Ghent University (UGent), Research Group of Sustainable Materials Science, Technologiepark 46, B-9052, Ghent, Belgium*

[c] *Mines Saint-Etienne, Univ Lyon, CNRS, UMR 5307 LGF, Centre SMS, F-42023, Saint-Etienne, France*

HIGHLIGHTS

- SKPFM was used to map the release of hydrogen through a Palladium covered surface.
- The impact of thermal oxides on the hydrogen release was investigated.
- Oxide layers resulted in a significant reduction in the release of hydrogen.
- FEM modelling was used to model lower diffusion and/or lower solubility in the oxide.

ARTICLE INFO

Article history:
Received 12 March 2023
Received in revised form
5 May 2023
Accepted 14 May 2023
Available online 1 June 2023

Keywords:
Hydrogen Embrittlement
Scanning Kelvin Probe Force Microscopy
Thermal Oxides
Finite Element Method

ABSTRACT

Scanning Kelvin Probe Force Microscopy (SKPFM) was used to study the hydrogen diffusion through a surface designed for simultaneous mapping of multiple areas containing different thermal oxides, all covered with Pd. Potential maps were obtained simultaneously on an area of bare iron as the reference, an area covered with a bilayer oxide (inner magnetite and outer hematite) and an area covered with a magnetite layer (obtained by removing the outer hematite layer of a bilayer oxide). After hydrogen charging at the bottom side of the specimen, a contrast was obtained in the potential mapping on the covering Pd layer due to differences in hydrogen release through these distinct areas on the specimen surface. A finite element method (FEM) model of hydrogen diffusion across the different phases was developed to simulate the experiment. The modelling showed that both a lower diffusion coefficient and a lower solubility in the oxide can explain the contrast obtained in SKPFM. Cross diffusion in the ferritic bulk underneath the thermal oxide was found to have an influence on the spatial distribution of the hydrogen release.

* *Corresponding author*. Department of Chemistry and Materials, Vrije Universiteit Brussel (VUB), Research Group of Electrochemical and Surface Engineering (SURF), Pleinlaan 2, 1050, Brussels, Belgium.
E-mail address: Tim.Rubben@vub.be (T. Rubben).

https://doi.org/10.1016/j.ijhydene.2023.05.142

Introduction

The problem of hydrogen assisted cracking (HAC) of steels has already been studied for decades, first being described more than 140 years ago [1]. However, further research is still required to obtain a full understanding of the problem. The presence of hydrogen in a metal can lead to an important loss of ductility, referred to as "hydrogen embrittlement (HE)". It can be difficult to determine the origin of the hydrogen, as it can be introduced during the production and processing or during the use of the material, respectively referred to as internal hydrogen embrittlement (IHE) and hydrogen environment embrittlement (HEE) [2]. It is generally agreed that, depending on the type of material and testing performed, multiple embrittlement mechanisms [3–9] may act simultaneously.

Multiple techniques have been used for the detection of hydrogen, such as electrochemical permeation, hot/melt extraction, thermal desorption spectroscopy and secondary ion mass spectroscopy [3,10]. Recently, the Kelvin probe has been used for the detection of hydrogen [3,10–14]. It has been reported that work function measurements can be used to detect hydrogen directly on steel. However, this was found to be difficult to reproduce [10,11,15]. Furthermore, steel (when unpolarized), is always covered by an oxide layer, which can vary in composition and thickness depending on the environmental conditions. As such, the work function of iron oxides could change due to hydrogen induced reduction of Fe^{3+} states to Fe^{2+} states [15], further complicating the procedure. Quantification was possible [13] but each type of oxide layer would require an individual calibration. Local inhomogeneities in the oxide could further aggravate this problem.

To alleviate this issue, a thin Pd layer can be deposited on top of the surface. The much lower chemical potential of hydrogen in Pd ensures direct entry of hydrogen from the surface into the Pd layer [10,11]. Locally higher releases of hydrogen across a surface then results in a locally higher hydrogen content in the Pd layer on top. Several studies [10,11,16] have shown that a change in hydrogen content within the Pd layer causes a shift in the measured potential (see Eq. (1)). The measured work function can be related to the H^+ concentration in the nanoscopic water layer adsorbed on the Pd layer, always present at ambient atmosphere, itself in equilibrium with the local hydrogen content in the Pd layer. As such, a higher hydrogen content in the Pd, resulting from a higher hydrogen release rate from the underlying material, becomes apparent as a lower potential on the surface [10]. By employing scanning Kelvin probe force microscopy (SKPFM), a microscale map of the local hydrogen release can be obtained [12,16].

$$E = E^{*}_{SHE} + \frac{RT}{F}\ln\left(\frac{a(H^+)}{a(H_{ab})}\right) \quad (1)$$

In a previous work [14], electrochemical and SKPFM experiments were performed to investigate the influence of pure magnetite and bilayer oxides (inner magnetite and outer hematite) on the hydrogen release out of a SAE1010 steel. For the SKPFM experiments, maps were scanned across a surface containing simultaneously the bare steel and one of the thermal oxides. A contrast in the potential was obtained, indicating a difference in hydrogen release for the different surfaces. Results showed that both types of thermal oxides were able to limit the diffusion out of the specimen. This was attributed to both a lower diffusion speed within the oxide and to the steel-oxide interface impeding the hydrogen transport, with the dominant factor changing depending on the type of thermal oxide. It should be noted that the pure magnetite and the bilayer oxides were investigated in separate experiments, which could have introduced variations due to changes in Pd thickness, hydrogen charging, tip used, etc.

For this reason, in the present work a dedicated specimen design was developed where different areas with different oxides are present on one and the same specimen. As such, different oxides were investigated in this work through scanning potential maps across a Pd covered surface containing simultaneously bare iron, bilayer oxide and magnetite (obtained by removing the outer hematite layer from a bilayer). In order to gain more insights into the mechanism of hydrogen diffusion through the oxide layers, Finite Element Method (FEM) modelling was conducted to provide a qualitative orientation in combination with the SKPFM experiment, taking into account the diffusion coefficient and solubility of the different phases. A modified Fick's equation [12] was used to account for a possible lower solubility in the oxide layer.

Experimental

Specimens

ARMCO® soft ingot iron specimens with a purity of 99.7% were used in this study. A diffusion coefficient of $4.76*10^{-11}$ m^2 s^{-1} was determined for this material in another work [17]. Square specimens with a side length of 1.5 cm and a thickness of 2 mm were prepared. The top surface of the specimens was ground with SiC-paper and polished with 1 μm grade diamond paste. Following this, the specimens were thermally oxidized in air atmosphere for 12 min at 250 °C. Afterwards, the bottom side of the specimens was ground with SiC-paper up to 800 grid in order to remove the thermal oxide on that side. According to the procedure of Wielant et al. [18,19], this thermal oxidation results in a bilayer oxide (inner magnetite and outer hematite) with a total thickness of 41 nm containing an outer hematite layer of only 4 nm thick. The composition and total thickness of the oxides were confirmed by Raman spectroscopy (not shown) and atomic force microscopy (AFM), respectively. Before use, specimens were ultrasonically cleaned in ethanol and dried in air.

The thermal oxide was further treated for use in SKPFM. Half of the oxidized surface was masked with 3M-tape 8402, followed by a complete dissolution of the non-masked section

of the thermal oxide in a citric acid solution (5 g/l). After removing the first mask, half of the remaining oxide was again masked, and the top few nm of the exposed oxide was removed by limiting the immersion time in the citric acid solution. This resulted in a surface containing sections of bare iron, bilayer oxide and magnetite (obtained by removing the outer hematite layer of a bilayer oxide). For the bare iron, an autonomously reformed oxide of a few nm could not be avoided due to the exposure of the samples to ambient air. After this sample surface preparation resulting into three different areas, a 8 nm Pd layer was deposited by physical vapor deposition using a PECS machine (20 mA for 90 s). A representation of the overall specimen preparation is shown in Fig. 1.

Scanning Kelvin probe force microscopy

Specimens were loaded with hydrogen on the reverse (without a thermal oxide) face through potentiostatic polarization at −1.2 V_{SCE} in a deaerated 30 g/l NaCl solution for 20 min. After charging, specimens were transferred to a commercial atomic force microscope (Nano-Wizard® 3 NanoScience AFM), introducing a delay of about 10 min. Based on the diffusion coefficient of this material ($4.76*10^{-11}$ m^2 s^{-1} [17]), the specimen was not saturated in hydrogen by the end of charging and only a limited amount of hydrogen would have reached the Pd layer. SKPFM measurements were conducted in ambient conditions using amplitude modulation detection and dual pass lift-up scan, with the topography being measured in tapping mode during the first pass. Scans were performed using a MIKROMASCH conductive silicon tip coated with platinum, with a resonant frequency and spring constant in the range of 60–100 kHz and 1.1–5.6 N/m, respectively. One full mapping took approximately 4 min, which could introduce a limited variation in the potential mapping due to release of hydrogen during the measurement. In order to map the release of hydrogen into the Pd layer, the procedure described in a previous work was adapted [14]. To achieve this, time-resolved potential maps were continuously scanned on a square area of 30 μm by 30 μm containing all three areas of interest - bare iron, bilayer oxide and magnetite - covered by Pd. As such, it was possible to acquire simultaneously the time evolution of the potential for the different areas, enabling a direct comparison of the hydrogen-diffusion through the different thermal oxides and the bare iron.

FEM modelling

A 2D finite element modelling of hydrogen diffusion across a specimen was conducted. For this, the model used by Tohme et al. [12] was adapted to include an oxide layer. A modified Fick's equation was used to account for multiphase systems with different diffusion coefficients and solubilities [12] (see Eq. (2)).Where C was the hydrogen concentration in molar fraction, S was the hydrogen solubility in molar fraction $bar^{-0.5}$, and D was the diffusion coefficient in m^2 s^{-1}. As such, the flux of hydrogen was governed by a chemical potential gradient instead of a concentration gradient, which was more representative for the multiphase systems [12].

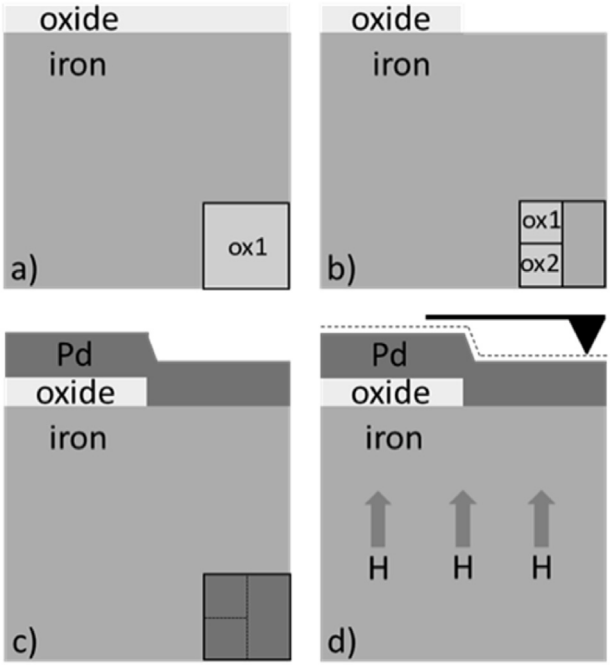

Fig. 1 – Cross-sectional view of the specimen preparation. It should be noted that the different layers were not drawn to scale. The square embedded in the lower right corner corresponded to the top view obtained after each step. a) Formation of a thermal oxide in air at 250 °C for 12 min. b) Masking of the surface with 3M-tape 8402 tape and (partial) removal of the oxide layer in citric acid solution, resulting in a surface containing bare iron (grey), unmodified bilayer oxide (ox 1, in light grey) and bilayer oxide with the outer hematite layer removed, leaving mainly magnetite (ox 2, in light grey). c) Deposition of a 8 nm thick Pd layer covering the complete specimen surface (dark grey). d) SKPFM mapping on top of the Pd layer covering the three types of surface.

$$S\frac{\partial\left(\frac{C}{S}\right)}{\partial t}=\nabla\left(DS\nabla\left(\frac{C}{S}\right)\right) \quad (2)$$

In this work, the model specimen consists of 3 phases: ferritic iron with half of its outer surface covered with an (non-specified) iron oxide and a Pd layer on top (see Fig. 2). In order to reduce the number of meshing elements, the modelled width was only 10 μm, which was in the order of magnitude that can be scanned with SKPFM. In the SKPFM experiments performed in this work, the width of the specimens was 1,5 cm, far exceeding the 2 mm thickness of the specimen. Consequently, release of hydrogen through the sides could be expected to be negligible compared to release through the charging or discharging surface. As such, isolated boundaries were imposed in the model at the sides of the specimen (see Fig. 2). Another isolated boundary was imposed on top of the Pd layer, disallowing hydrogen release through this surface as well. In reality, some loss of hydrogen from the Pd layer is possible due to reaction with oxygen, as was reported for SKPFM experiments performed in air [10,11,20–22]. However,

in other works [12,14], the loss of hydrogen was found to not have a significant impact on the resulting potential contrast, demonstrating limited release of hydrogen through the Pd surface. This may be related to the nanocrystalline nature of the deposited Pd layer leading to very low diffusion of hydrogen to the surface, as was observed from limited cross-diffusion in other works [12]. As the main goal was to qualitatively compare the possible impact of a lower diffusion coefficient and/or solubility in the oxide, the assumption of no release of hydrogen through the Pd surface was made to simplify the model.

A fugacity f of hydrogen was imposed on the left (charging) surface (see Fig. 2), giving a surface concentration C_S according to Sieverts's law [23] (see Eq. (3)). The fugacity was first set to 100 bar during the 20 min of hydrogen charging and afterwards set to 0 bar. As a result, hydrogen could leave through the charging surface after the end of charging.

$$C_s = S\sqrt{f} \tag{3}$$

A diffusion coefficient of $4.76*10^{-11}$ m^2 s^{-1} was used for the bulk material, as determined for this material in a different work [17]. As the microstructure was ferritic, a solubility of $2.8*10^{-8}$ M fraction $bar^{-0.5}$ was used [24,25]. The diffusion coefficient and solubility in the Pd layer were taken from another work [12], respectively chosen as being $1*10^{-18}$ m^2 s^{-1} and 0.1 M fraction $bar^{-0.5}$. These respectively low and high values of diffusivity and solubility of hydrogen in palladium are justified by the highly defective nature of the deposited Pd layer [12]. The effect of the presence of an oxide layer was modelled by considering a lower diffusion coefficient and/or a lower solubility in the oxide layer compared to in the bulk ferrite. To separate the contribution of these parameters, the effect of these parameters was investigated both separately and simultaneously. For this, a diffusion coefficient of 10^{-19} m^2 s^{-1} [26] and/or a solubility of 10^{-11} M fraction $bar^{-0.5}$ was considered. The parameters used in the model are listed in Table 1.

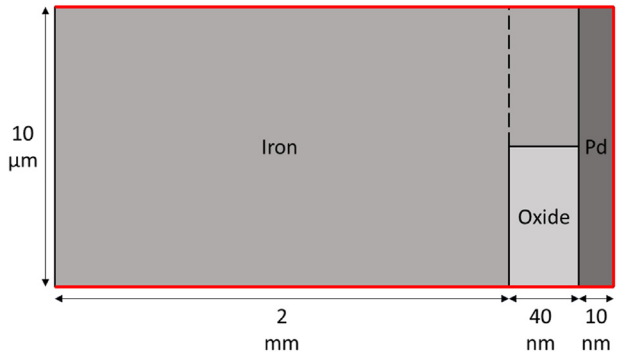

Fig. 2 – Representation of the different dimensions and phases of the specimen used in the FEM modelling. The modelled area represents a cross-section of the specimen scanned with SKPFM. Each phase had its own diffusion coefficient D and solubility S. The red lines at the top, bottom and right side indicate the presence of an isolated boundary in the model, disallowing hydrogen transport across these surfaces. (For interpretation of the references to colour in this figure legend, the reader is referred to the Web version of this article.)

Results

Scanning Kelvin probe force microscopy analysis

In order to monitor the release of hydrogen, potential maps were scanned on regions containing simultaneously bare iron (with native oxide), bilayer oxide and magnetite. A topography map obtained before Pd deposition and a selection of potential maps obtained at different times after the start of the 20 min of charging are shown in Fig. 3. Three distinct zones were observed in the topography map (see Fig. 3a): the bilayer oxide on the top right, the magnetite on the bottom right and the bare iron on the left. Fig. 3b shows examples of topography line profiles obtained between the bare iron and the bilayer oxide, and between the bilayer oxide and the magnetite. An average step height of 5 nm was obtained between the unmodified bilayer oxide and the magnetite, which indicated that the outer hematite layer was removed [18,19]. Before charging, a mostly uniform distribution in potential was obtained across all surfaces (see Fig. 3c). As such, no influence on the CPD was expected from the underlying oxide since the surface potentials measured corresponded to those of the Pd layer [14]. Therefore, any CPD changes with time after H-charging was to the accumulation of hydrogen in the Pd layer. After charging, a continuous decrease in potential with time could be noted for all areas on the sample, indicating that hydrogen was being continuously released. Furthermore, a clear contrast was seen immediately between the bare iron and the oxidized areas (see Fig. 3d–f). Additionally, a slight contrast was observed between the bilayer oxide and the magnetite. As such, the highest potential was obtained for the bilayer oxide, followed by the magnetite and finally the bare iron. This indicated firstly that less hydrogen was released into the Pd layer (see Eq. (1)) when a thermal oxide (bilayer or magnetite) was present underneath, and secondly that the presence of the thin outer hematite layer in the bilayer oxide impedes the hydrogen transport even further compared to only having a magnetite layer.

To better demonstrate the difference between the two types of oxide, the average potential values were calculated

Table 1 – Parameters used in the modelling.

Parameter	Value
Total simulation time	12,000 s
# meshing elements	30,816
# boundary meshing elements	13,538
Diffusion coefficient in the bulk	$D_b = 4.76*10^{-11}$ m^2 s^{-1} [17]
Diffusion coefficient in palladium	$D_{Pd} = 1*10^{-18}$ m^2 s^{-1} [12]
Diffusion coefficient in the oxide	$D_{ox} = 1*10^{-19}$ m^2 s^{-1} [26]
Solubility in the bulk	$S_b = 2.8*10^{-8}$ M fraction $bar^{-0.5}$ [24,25]
Solubility in palladium	$S_{Pd} = 0.1$ M fraction $bar^{-0.5}$ [12]
Solubility in the oxide	$S_{ox} = 1*10^{-11}$ M fraction $bar^{-0.5}$
Fugacity during charging	f = 100 bar

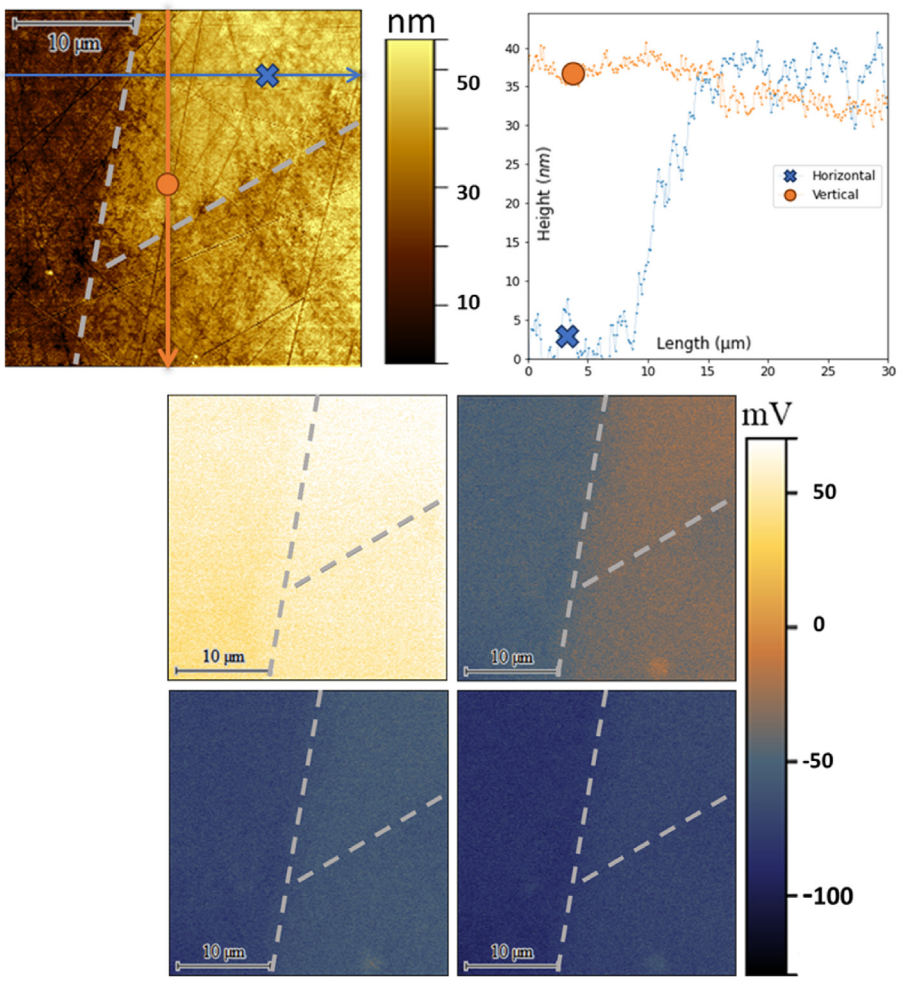

Fig. 3 – Results obtained through scanning a 30 µm × 30 µm section containing simultaneously the bare iron (left), the unmodified bilayer oxide (top right) and the magnetite oxide (bottom right). The dotted lines mark the edges of the different areas. a) Topography map obtained before deposition of the Pd layer and b) the corresponding line profiles obtained across the bare iron - bilayer oxide edge (horizontal line) and across the full oxide (bilayer) - partial oxide (magnetite) edge (vertical line). Potential maps were obtained on the surface after the Pd layer was deposited. A selection is shown corresponding to c) 0 min s, d) 30 min, e) 60 min, and f) 90 min after the start of the 20 min of charging.

for the bare iron, bilayer oxide and magnetite (see Fig. 4). A potential decrease with time was noticed for all three types of surface conditions, pointing to an accumulation of hydrogen in the Pd layer (see Eq. (1)). A smaller overall decrease in potential was obtained for the surfaces with a thermal oxide, pointing towards a slower release of hydrogen through an oxidized surface, as was seen in a previous study [14]. This effect appeared to be more pronounced for the bilayer, which showed the largest difference compared to the blank surface.

FEM modelling

Fig. 5 shows the time evolution of the bulk hydrogen distribution for a specimen without an oxide layer, calculated from FEM modelling. It can be seen that hydrogen moved deeper in the material over time, with a very small amount of hydrogen already present at the exit surface (x = 2 mm) 10 min after the end of charging (Time = 1800s)), which can be more clearly seen in a later figure. This matched the results obtained with SKPFM (see Fig. 3), where hydrogen could be detected immediately after charging. The effect of a lower diffusion speed and/or a lower solubility in the oxide layer was also modelled. Fig. 6 shows the hydrogen distribution near the iron-oxide interface for the different conditions (see Fig. 6a), corresponding to 2 h after the start of the 20 min of charging. Note that the hydrogen concentration was represented using a logarithmic colour scale, as the potential measured on Pd depends on the logarithm of the hydrogen concentration in the Pd layer (see Eq. (1)). In all cases, an accumulation of hydrogen in the Pd layer was observed. As expected, in the case that there was no thermal oxide (see Fig. 6b, $D_{ox} = D_b$, $S_{ox} = S_b$), a uniform concentration of hydrogen in the Pd layer was predicted. A clear contrast within the Pd layer was obtained by considering an oxide layer on part of the surface

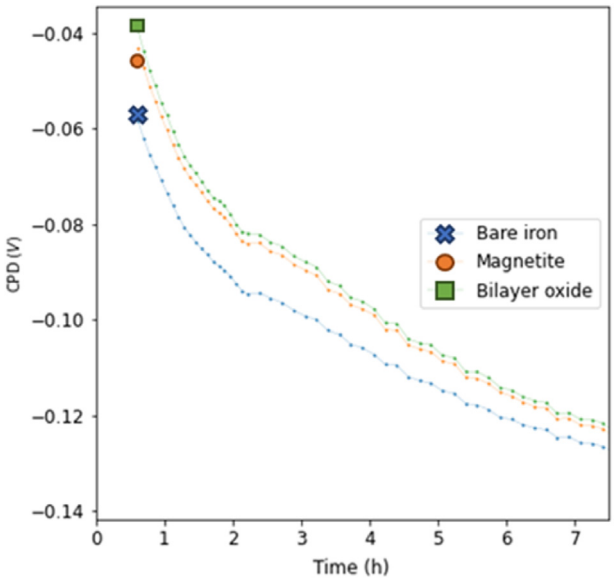

Fig. 4 – Time evolution of the average potential of the different surfaces shown in Fig. 3. The bare iron (blue cross), the unmodified bilayer oxide (green square)and the magnetite oxide (green square, obtained by removing the outer hematite layer from the bilayer oxide) can be seen. (For interpretation of the references to colour in this figure legend, the reader is referred to the Web version of this article.)

with a lower diffusion coefficient (see Fig. 6c, $D_{ox} = 1*10^{-19}$ m^2 s^{-1}, $S_{ox} = S_b$). Consequently, a lower hydrogen content was obtained in the Pd above the oxide layer, showing the ability of the oxide to limit the hydrogen diffusion.

A similar result was obtained when considering an oxide layer with a lower solubility (see Fig. 6d, $D_{ox} = D_b$, $S_{ox} = 1*10^{-11}$ M fraction $bar^{-0.5}$), pointing to the possibility of having a barrier effect due to a sharp drop in solubility at the iron-oxide interface [14,27]. Additionally, a clearly lower hydrogen content within the oxide layer itself was observed, resulting from the decreased solubility. An interplay of the two mechanisms can also result in the contrast (see Fig. 6e, $D_{ox} = 1*10^{-19}$ m^2 s^{-1}, $S_{ox} = 1*10^{-11}$ M fraction $bar^{-0.5}$). It should be noted that a limited cross-diffusion of hydrogen within the Pd layer itself was seen near the iron-oxide edges. Line profiles showing the time evolution of the hydrogen concentration at several locations (see dotted lines in Fig. 6a) were plotted in Figs. 7 and 8. Fig. 7 shows the hydrogen concentration in the bulk, 100 nm below the Pd layer, for material without (see Fig. 7a) and with a 40 nm oxide layer covering half the surface (see Fig. 7b). Uniform concentrations were found for the specimens without an oxide layer. When an oxide layer was present, a concentration gradient was obtained with a higher concentration of hydrogen underneath the oxide layer. This gradient evened out in time, leading to an overall higher concentration than when no oxide layer was present (see Fig. 7a vs Fig. 7b), pointing towards the importance of cross-diffusion within the bulk of the material.

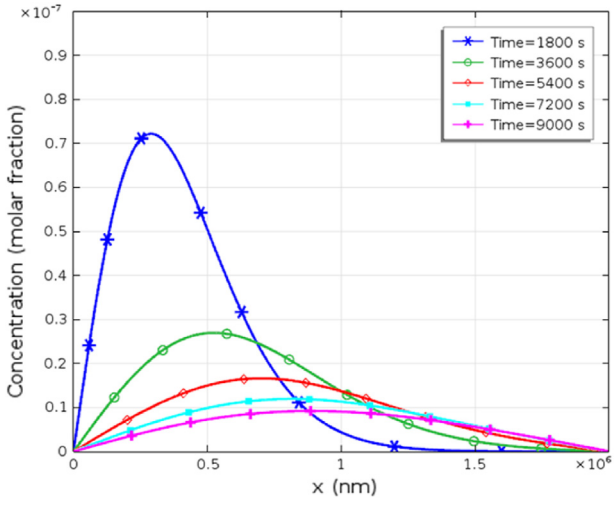

Fig. 5 – Results of the FEM modelling showing the evolution of the concentration in the bulk for a specimen without an oxide.

Fig. 8 shows the time evolution of the hydrogen content within the Pd layer for material without (see Fig. 8a) and with (see Fig. 8b) an oxide layer covering half the surface. An accumulation of hydrogen in the Pd layer was obtained in all cases, although the hydrogen concentration was lower in the Pd above the oxide layer. The contrast in concentration was immediately visible when an oxide layer was present (see Fig. 8b). Additionally, a limited cross-diffusion of hydrogen within the Pd layer was observed, which has been observed before in SKPFM experiments [10,12]. By comparing the hydrogen content for the different conditions, it was seen that a higher local hydrogen concentration was obtained above the bare iron when a thermal oxide was added to part of the surface. A direct comparison of concentration, plotted in a linear instead of a logarithmic scale, is shown in Fig. 9. These results showed that hydrogen was still able to somewhat "circumvent" the oxide layer, which has important implications for the quantity of hydrogen that is released through the different surfaces.

Discussion

Specimens were investigated by scanning potential maps on the exit surface with SKPFM. It should be noted that specimen transfer introduced a delay of about 10 min between the end of charging and the start of potential mapping. As a contrast was immediately visible after the charging, hydrogen was already being released into the Pd layer, resulting in a change of CPD. Fig. 3 showed a decrease in time for the Volta potential, corresponding to an accumulation of hydrogen in the Pd layer (see Eq. (1)) due to hydrogen release out of the specimen [11]. It should be noted that the overall drop in potential cannot be compared to the drop in a previous work [14], due to different Pd layer thickness, specimen thickness and charging conditions, underlining the importance of performing a direct comparison. It has been reported by Evers et al. [10,11] that some loss of hydrogen out of the Pd layer could have occurred due to reaction with oxygen. However, as no increase in potential was obtained within the measured timeframe (see Fig. 4), any loss seemed to have been low compared to the

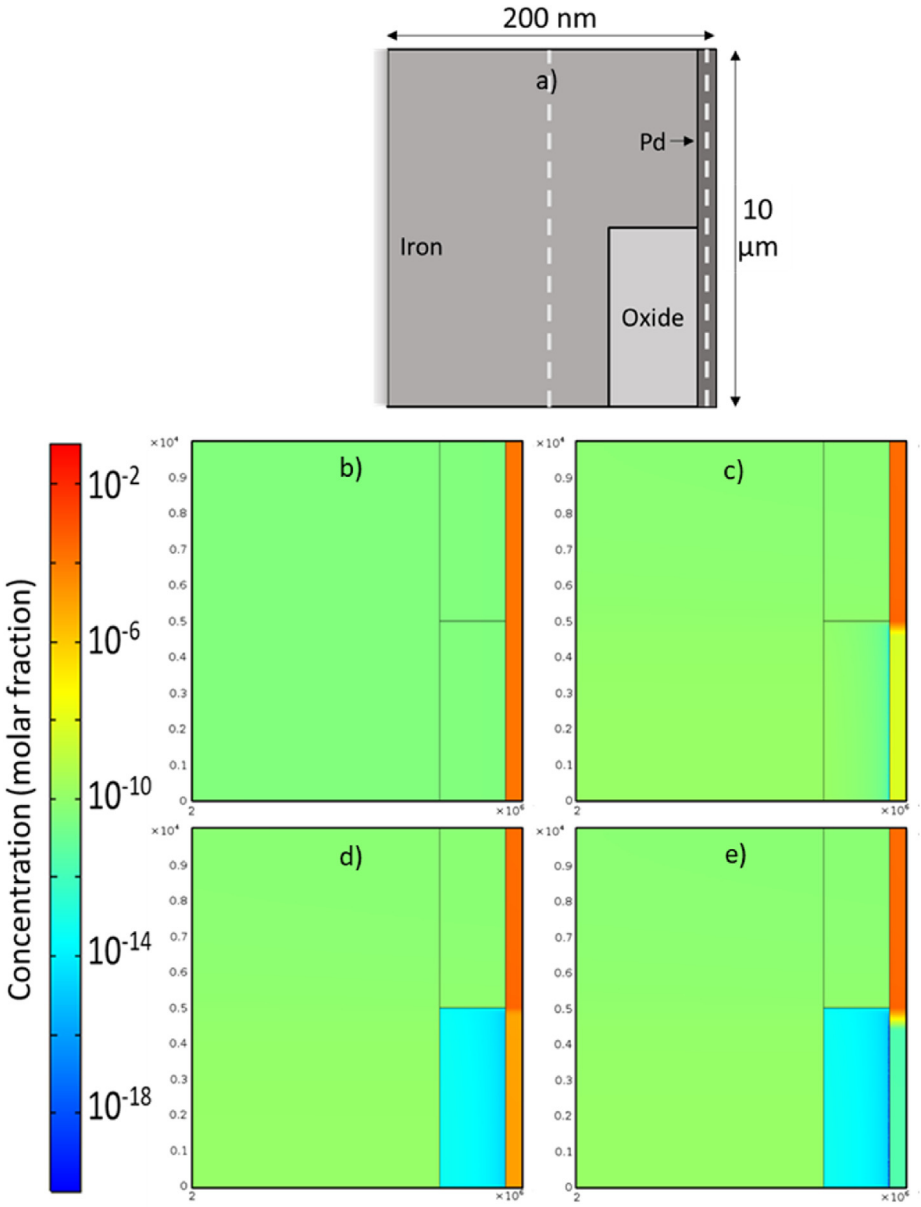

Fig. 6 – Results of the FEM modelling showing the effect of different parameters in the oxide, 2 h after the start of the 20 min of charging. a) Representation of the plotted figure showing the dimensions and the different phases. Note that only the top 200 nm of the specimen, including the oxide and Pd layers, was plotted. b) no oxide ($D_{ox} = D_b$, $S_{ox} = S_b$), c) a lower diffusion coefficient in the oxide ($D_{ox} = 1*10^{-19}$ m^2 s^{-1}, $S_{ox} = S_b$), d) a lower solubility in the oxide ($D_{ox} = D_b$, $S_{ox} = 1*10^{-11}$ M fraction $bar^{-0.5}$), d) both a lower solubility and lower diffusion coefficient in the oxide ($D_{ox} = 1*10^{-19}$ m^2 s^{-1}, $S_{ox} = 1*10^{-11}$ M fraction $bar^{-0.5}$).

release of hydrogen into the Pd layer. Additionally, no significant loss of hydrogen from the Pd layer was found in some other works [12,14] for SKPFM experiments performed in air. A cause for this disparity could be the use of different materials, charging conditions and Pd layer characteristics (thickness, microstructure, deposition conditions) [14]. Regardless, any loss of hydrogen would have mainly had an impact on quantification whilst in this work a qualitative comparison was performed. Also in the model, no loss of hydrogen from the Pd layer was considered.

The thermally oxidized areas showed a higher potential compared to the blank area, indicating that less hydrogen was released through these oxides into the Pd (see Fig. 4). This indicated that the bilayer oxide (inner magnetite and outer hematite) effectively limited the diffusion. This may be attributed to a lower diffusion speed of hydrogen in the oxide [26,28] as it would cause hydrogen to take a longer time to reach the Pd layer. The oxide-iron interface may have a contributing impact as well, as shown in a previous work [14]. Both possible contributions were investigated through the

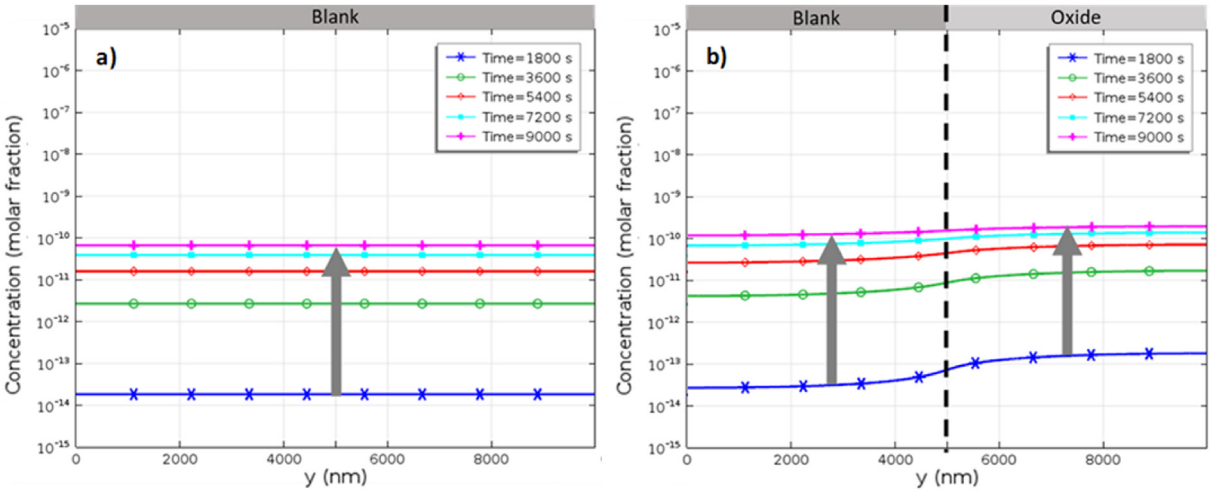

Fig. 7 – Concentration profile underneath the oxide, after the start of the 20 min of charging. The profile corresponds to the leftmost dotted line in Fig. 6a. The figures correspond to a) the case of no oxide, b)the case of an oxide with both a lower D and a lower S.

modelling (see below). By removing the top surface of the oxide, a larger release of hydrogen was obtained despite the small change in overall oxide thickness (see Fig. 4). This was attributed to the removal of the more insulating outer hematite layer [14], pointing towards the importance of a lower diffusion coefficient in this thin removed layer of oxide.

FEM modelling was used to investigate the effect of a lower diffusion coefficient and/or of a lower solubility in the oxide layer on the distribution of hydrogen in the Pd layer. In a previous experimental study, the steel/oxide interface was found to have a strong effect for pure magnetite layers [14], while the lower diffusion speed proved dominant in the case of magnetite layers enriched with Cr on low Cr-low Ni stainless steel. The modelling performed in this work demonstrated that both a lower diffusion speed in the oxide (see Fig. 6c), and a diffusion barrier effect due to a sharp drop in solubility at the iron-oxide interface [27] (see Fig. 6d) can produce the contrast observed with SKPFM (see Fig. 3c–f). It is likely that both factors contributed to limiting the diffusion through the oxide, with the dominant factor changing depending on the specific properties of the oxide.

The modelling showed that the presence of an oxide layer caused less hydrogen to reach the Pd layer (see Figs. 6 and 8), resulting in a higher concentration directly underneath the oxide layer (see Fig. 7b). Furthermore, cross diffusion within the ferrite underneath the oxide led to a higher hydrogen concentration underneath the adjacent blank surface compared to when there was no oxide present on the surface (see Fig. 7 a vs b). Consequently, more hydrogen remained available to enter the Pd layer through the blank surface,

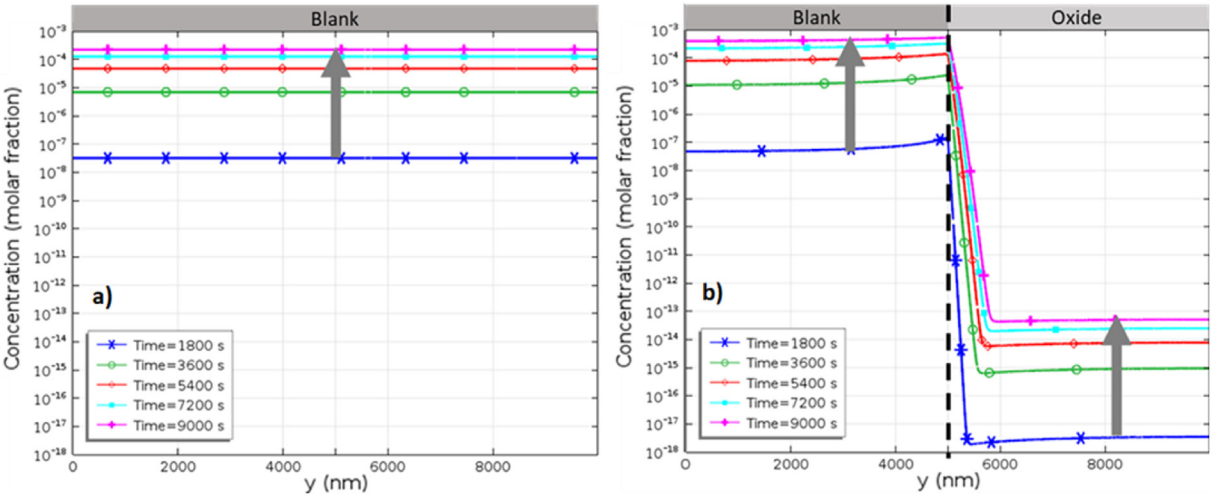

Fig. 8 – Concentration profile in the Pd layer, after the start of the 20 min of charging. The profile corresponds to the rightmost dotted line in Fig. 6a. The figures correspond to a) the case of no oxide, b)the case of an oxide with both a lower D and a lower S.

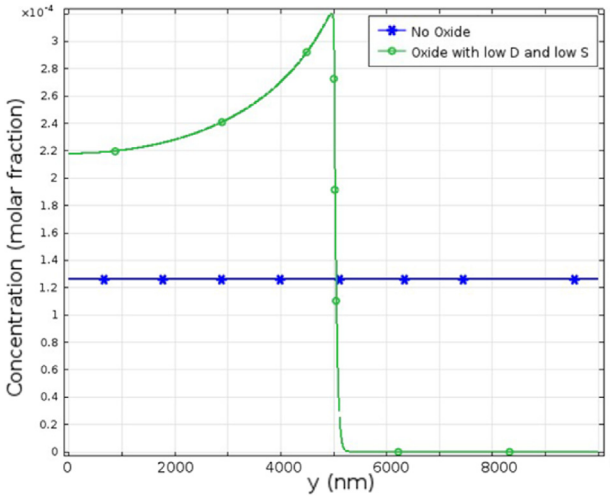

Fig. 9 – Concentration profile in the Pd layer, 2 h after the start of the 20 min of charging. A linear scale was used to better exemplify the effect of the oxide on the hydrogen release into the Pd layer. The blue (cross) and green (circle) profiles in this figure correspond to the light blue (circle) lines in Fig. 8a and b, respectively. (For interpretation of the references to colour in this figure legend, the reader is referred to the Web version of this article.)

leading to a higher concentration in the Pd layer above the blank surface compared to when there was no oxide present adjacent to it (see Fig. 8 a vs b). As such, cross-diffusion within the bulk material could have a noticeable impact on the obtained contrast in the Pd layer when directly comparing areas with/without oxide layers. It can be expected that for materials with a lower diffusion coefficient in the bulk (e.g. austenite) and for experiments where continuous charging is performed, this effect would be mitigated. Regardless, this effect would mainly be important when performing a quantitative comparison (see Fig. 9). A qualitative comparison can still be performed, as evidenced in Fig. 6, where clear distinctions were made for the different oxide types.

It should be noted that the calculated values are only meant to provide a qualitative orientation. The simplifications that were made likely lead to errors in the obtained values. Furthermore, the obtained values were not directly verified with the experimental results as the exact concentration of hydrogen in the Pd layer during the experiment was not known (The change in potential with concentration can vary from the theoretical 60 mV per decade for nanocrystalline Pd layers [11,29]). Regardless, these factors would not qualitatively affect the conclusions.

Conclusion

A SKPFM based methodology was used to monitor the release of hydrogen through a Pd-covered specimen where in the same scanned region there was simultaneously an area of bare iron, an area with unmodified thermal bilayer oxide and an area with a partially removed thermal oxide, leaving magnetite. FEM modelling was conducted to simulate and support the SKPFM experiment, taking into account the possible effect of a lower diffusion coefficient and/or a lower solubility in the oxide layer. The findings of this study are summarized as follows.

- A clear contrast in potential was obtained for the different areas, showing that the SKPFM based methodology can be used to directly compare the hydrogen release through multiple areas with different surface layers.
- Removal of the thin outer hematite layer of a thermal bilayer, leaving magnetite, led to a noticeable difference in potential. This was despite the total oxide thickness decreasing by only a few nm, showing the importance of this thin outer hematite layer for limiting the release of hydrogen.
- Modelling showed that both a lower diffusion speed and a lower solubility of hydrogen within the oxide can be responsible for the contrast observed through SKPFM.
- The modelling demonstrated that cross-diffusion underneath the oxide layer could have an important influence on the distribution of the hydrogen release. This did not pose a problem for the qualitative comparison performed in this work but could have important implications if a quantitative comparison is to be performed.

Declaration of competing interest

The authors declare that they have no known competing financial interests or personal relationships that could have appeared to influence the work reported in this paper.

Acknowledgments

The authors gratefully acknowledge AVN (Association Vinçotte Nuclear) for the financial support of this PhD project. Furthermore, the authors acknowledge support from FWO (senior postdoctoral fellow grant 12ZO420 N). The authors would also like to thank Bart Lippens for polishing the specimens.

REFERENCES

[1] Johnson WH. On some remarkable changes produced in iron and steel by the action of hydrogen and acids. Proc R Soc London 1875;23:168–79.
[2] Symons DM. A comparison of internal hydrogen embrittlement and hydrogen environment embrittlement of X-750. Eng Fract Mech 2001;68:751–71.
[3] Rudomilova D, Prošek T, Luckeneder G. Techniques for investigation of hydrogen embrittlement of advanced high strength steels. Corrosion Rev 2018;36:413–34. https://doi.org/10.1515/corrrev-2017-0106.

[4] Troiano AR. The role of hydrogen and other interstitials in the mechanical behaviour of metals. Trans. ASM. 1960;52:54–80.
[5] Beachem CD. A new model for hydrogen-assisted cracking. Met. Trans. A. 1972;3:437–51.
[6] Birnbaum P, Sofronis HK. Hydrogen-enhanced localized plasticity—a mechanism for hydrogen-related fracture. Mater Sci Eng 1994;176:191–202.
[7] Nagumo M. Hydrogen related failure of steels – a new aspect. Mater Sci Technol 2004;20:940–50. https://doi.org/10.1179/026708304225019687.
[8] Depover T, Verbeken K. The detrimental effect of hydrogen at dislocations on the hydrogen embrittlement susceptibility of Fe-C-X alloys: an experimental proof of the HELP mechanism. Int J Hydrogen Energy 2018;43:3050–61. https://doi.org/10.1016/j.ijhydene.2017.12.109.
[9] Lynch S. Hydrogen embrittlement phenomena and mechanisms. Corrosion Rev 2012;30:105–23. https://doi.org/10.1515/corrrev-2012-0502.
[10] Evers S, Senöz C, Rohwerder M. Hydrogen detection in metals: a review and introduction of a Kelvin probe approach. Sci Technol Adv Mater 2013;14. https://doi.org/10.1088/1468-6996/14/1/014201.
[11] Evers S, Rohwerder M. The hydrogen electrode in the dry: a Kelvin probe approach to measuring hydrogen in metals. Electrochem Commun 2012;24:85–8. https://doi.org/10.1016/j.elecom.2012.08.019.
[12] Tohme E, Barnier V, Christien F, Bosch C, Wolski K, Zamanzade M. SKPFM study of hydrogen in a two phase material. Experiments and modelling. Int J Hydrogen Energy 2019;44:18597–605. https://doi.org/10.1016/j.ijhydene.2019.05.177.
[13] Nazarov A, Vucko F, Thierry D. Scanning Kelvin Probe for detection of the hydrogen induced by atmospheric corrosion of ultra-high strength steel. Electrochim Acta 2016;216:130–9. https://doi.org/10.1016/j.electacta.2016.08.122.
[14] Rubben T, Baert K, Depover T, Verbeken K, Revilla RI, De Graeve I. Influence of thermal oxide layers on the hydrogen transport through the surface of SAE 1010 steel. J Electrochem Soc 2022;169:111503. https://doi.org/10.1149/1945-7111/aca182.
[15] Krasemann M, Streckel H, Hoffmann K, Grabke H-J, Stratmann M. Detection of hydrogen ingress into iron oxide and iron oxy-hydroxide layers by the Kelvin probe. In: Proc. Symp. Passiv. Its break; 1998. p. 207–20. File:///D:/Download/s10008-017-3541-3.pdf, File:///D:/Download/1-s2.0-0010938X89901236-main.pdf.
[16] Evers S, Senöz C, Rohwerder M. Spatially resolved high sensitive measurement of hydrogen permeation by scanning Kelvin probe microscopy. Electrochim Acta 2013;110:534–8. https://doi.org/10.1016/j.electacta.2013.04.171.
[17] Vecchi L, Simillion H, Montoya R, Van Laethem D, Van den Eeckhout E, Verbeken K, Terryn H, Deconinck J, Van Ingelgem Y. Modelling of hydrogen permeation experiments in iron alloys: characterization of the accessible parameters - Part I - the entry side. Electrochim Acta 2018;262:153–61. https://doi.org/10.1016/j.electacta.2017.12.173.
[18] Wielant J, Goossens V, Hausbrand R, Terryn H. Electronic properties of thermally formed thin iron oxide films. Electrochim Acta 2007;52:7617–25. https://doi.org/10.1016/j.electacta.2006.12.041.
[19] Goossens V, Wielant J, Van Gils S, Finsy R, Terryn H. Optical properties of thin iron oxide films on steel. Surf Interface Anal 2006;38:489–93. https://doi.org/10.1002/sia.2219.
[20] Zhong X, Schulz M, Wu CH, Rabe M, Erbe A, Rohwerder M. Limiting current density of oxygen reduction under ultrathin electrolyte layers: from the micrometer range to monolayers. Chemelectrochem 2021;8:712–8. https://doi.org/10.1002/celc.202100083.
[21] Vijayshankar D, Altin A, Merola C, Bashir A, Heinen E, Rohwerder M. Probing the buried metal-organic coating interfacial reaction kinetic mechanisms by a hydrogen permeation based potentiometric approach. J Electrochem Soc 2016;163:C778–83. https://doi.org/10.1149/2.0971613jes.
[22] Vijayshankar D, Tran TH, Bashir A, Evers S, Rohwerder M. Hydrogen permeation as a tool for quantitative characterization of oxygen reduction kinetics at buried metal-coating interfaces. Electrochim Acta 2016;189:111–7. https://doi.org/10.1016/j.electacta.2015.12.030.
[23] Sieverts A. Absorption of gases by metals. Zeitschrift Für Met. 1929;21:37–46.
[24] Turnbull A, Hutchings RB. Analysis of hydrogen atom transport in a two-phase alloy. Mater Sci Eng 1994;177:161–71. https://doi.org/10.1016/0921-5093(94)90488-X.
[25] Kiuchi K, McLellan RB. The solubility and diffusivity of hydrogen in well-annealed and deformed iron. Acta Metall 1983;31:961–84. https://doi.org/10.1016/0001-6160(83)90192-X.
[26] Vecchi L, Pecko D, Van den Steen N, Haile Mamme M, Ozdirik B, Van Laethem D, Van Ingelgem Y, Deconinck J, Terryn H. A modelling approach on the impact of an oxide layer on the hydrogen permeation through iron membranes in the Devanathan-Stachurski cell. Electrochim Acta 2018;286:139–47. https://doi.org/10.1016/j.electacta.2018.08.022.
[27] Schmitz G, Yang QM, Kesten P, Geyer U, Hülsen UV, Reimann K, Kirchheim R. Diffusion of hydrogen in metallic multilayers, Defect Diffus. Forum 1997;143–147:945–50. https://doi.org/10.4028/www.scientific.net/DDF.143-147.945.
[28] Vecchi L, Simillion H, Montoya R, Van Laethem D, Van den Eeckhout E, Verbeken K, Terryn H, Deconinck J, Van Ingelgem Y. Modelling of hydrogen permeation experiments in iron alloys: characterization of the accessible parameters - Part I - the entry side. Electrochim Acta 2018;262:57–65. https://doi.org/10.1016/j.electacta.2017.12.173.
[29] Mütschele T, Kirchheim R. Hydrogen as a probe for the average thickness of a grain boundary. Scripta Metall 1987;21:1101–4. https://doi.org/10.1016/0036-9748(87)90258-4.